Processes of Solar Radiation Transfer
Through a Sub-Arctic Shrub Canopy

DAN BEWLEY[1], JOHN W. POMEROY[1,2], AND RICHARD L.H. ESSERY[1]

ABSTRACT

Much of the low Arctic is covered with shrub tundra. Snowmelt energy exchange under shrub canopies is strongly influenced by the transmission of shortwave radiation through the canopy and the reflectance from snow under the canopy. Tundra shrub canopies are distinctive in that they are partially buried in winter and become exposed during snowmelt as snow depth decreases. The objectives of this study were to measure and model shortwave radiation reflection and extinction by one such dynamic heterogeneous deciduous shrub canopy over a melting snowcover. Observations were made in tundra shrub canopies of varying height in the mountains of the Yukon Territory, Canada. Measurements were taken over the course of spring snowmelt, during which solar elevation was low to moderate and the fractional area of exposed shrub overlying snow increased three-fold. Shrubs shaded most of the snow surface at low solar elevation angles, therefore a large component of shortwave radiation never reached the snow surface but was extinguished by the shrub canopy. At higher solar angles there was greater direct shortwave transmission to the snow surface between shrubs. A simple model was developed to incorporate this changing shade factor contribution to the overall shortwave transmissivity of shrub canopies. The model simulates both the landscape-averaged (areal) transmission and reflection of shortwave radiation, and results indicate that areal transmissivity and reflection can be up to 0.70 and 0.61 lower, respectively, relative to that simulated by a two-stream approximation in which no shadows are cast. A simple parameterization of this shaded landscape fraction is then proposed with which to integrate into hydrological and land surface models, for the purpose of simulating more accurately the melt rate and atmospheric fluxes in other areas of shrub tundra.

Key Words: shortwave radiation, transmissivity, albedo, extinction, snowmelt, shrub tundra, mountain snowcover, Yukon, Arctic

INTRODUCTION

Shrub vegetation coexists with seasonal snow cover over much of the sub-arctic region, and forms the dominant land cover over northern Alaska, the Canadian low Arctic, and parts of Siberia (DeFries *et al*., 1998). Sturm *et al*. (2001) present evidence from historical and modern photographs of increasing shrub abundance in arctic Alaska; this evidence is further supported throughout the pan-Arctic by a number of satellite remote sensing studies (e.g. Jia *et al*., 2003).

[1] Centre for Glaciology, Institute of Geography and Earth Sciences, University of Wales, Aberystwyth, Wales, UK, SY23 3DB.
[2] Centre for Hydrology, Dept of Geography, University of Saskatchewan, 117 Science Place, Saskatoon, Saskatchewan, Canada, S7N 5C8

Two of the three fastest warming regions on the planet in the last few decades have been Alaska and Siberia (NERC, 2005), and Epstein *et al*. (2004) suggest that the shrubs characterizing the transitional area between shrub-tundra and tussock-tundra, are sensitive indicators of climate warming and appear to be the most responsive ecosystem to climatic warming over a wide range of tundra and treeline biomes considered.

The melt rates of snow in shrub tundra may be substantially different from that in sparse tundra (Pomeroy *et al*., this issue), in addition to the disparity in snow depths observed by Sturm *et al*. (2005) as taller shrubs trap more snow. Pomeroy and Granger (1997) showed early results of the increase to net radiation during melt as dark shrubs in boreal forest clearings became progressively exposed through the thinning snowpack, which allows for both greater longwave radiation emission and upward sensible heat flux (Lee and Mahrt, 2004). Both Strack *et al*. (2003) and Viterbo and Betts (1999) found that weather model simulations were too cold (by as much as 6°C) when the role of vegetation over snow was not represented correctly. High melt rates and melt quantities from shrub tundra have been shown to control the timing of streamflow discharge in tundra basins (McCartney *et al*., this issue), and in atmospheric models, the melt rates have important implications for the calculated fractional snow covered area (Essery and Pomeroy, 2004), which in turn strongly influences the albedo, net radiation and surface fluxes of sensible heat and water vapour.

Sub-arctic shrub tundra consists primarily of open to closed canopy alder or birch-willow shrubs (Jorgenson and Heiner, 2004). Closed shrub canopies are represented in land surface models as a homogenous vegetation cover, and the shortwave radiative transfer algorithms associated with this canopy may be highly simplistic (e.g. Raupach *et al*., 1997). Whilst dual source schemes exist to parameterize the heterogeneity in land cover associated with an open shrub canopy (e.g. Huntingford *et al*, 1995; Blyth *et al*., 1999), these have been developed for arid or semi-arid areas in which the vegetated fractional coverage and density is relatively constant over time. These schemes also commonly employ the two-stream approximation when simulating shortwave radiation transfer through this landscape, in which it is assumed that the sun is located at an overhead position and no shadows are cast across the landscape. Gryning *et al*. (2001) demonstrated that the heat flux of a sparse coniferous forest is actually controlled more by the shading effect of the trees, and is not very sensitive to the actual fraction of surface occupied by forest.

In contrast to the model simplicity associated with a continuous canopy coverage, a number of complex physically-based models such as GORT (Ni *et al*. 1997) and TSETSE (Roujean, 1999) have been developed to simulate the processes of shortwave radiation transmission and reflection through an open canopy in forested catchments (e.g. Koivusalo and Kokkonen, 2002; Woo and Giesbrecht, 2000). These commonly use a combination of geometrical optics and radiative transfer schemes to account for extinction by canopy elements and the influence of canopy gaps on transmittance through the canopy. However, these models require a number of parameters that are not routinely measured as part of forest inventory descriptions (Nijssen and Lettenmaier, 1999), and their application is limited to highly focused research investigations. A similar study of the radiation attenuation within deciduous sub-arctic shrub canopies, of much lower foliage, density, continuity and height, has yet to occur and forms the focus of the current study.

It is the purpose of this paper to:
− improve the understanding of shortwave radiation transmission through and reflection from deciduous sub-arctic shrub canopies;
− develop a simple dual source radiative transfer model to simulate the areal transmissivity of shortwave radiation through and albedo above an emerging discontinuous deciduous canopy;
− study the influence of solar elevation angle on shortwave transmission and albedo at both the individual bush scale, and at the landscape scale where canopy extinction of shortwave radiation occurs in the shrub shaded areas; and
− develop a simple parameterization of the shaded fractional area, requiring only simple statistics of the shrub canopy, that may be applied in distributed hydrological models and land surface representations of climatological models.

FIELD SITES AND MEASUREMENTS

Field measurements were conducted in the 195 km^2 Wolf Creek Research Basin (60°35' N, 135°11' W) near Whitehorse, Yukon Territory. Wolf Creek Research Basin lies in the southern mountainous headwaters of the Yukon River Basin in the sub-arctic of northwestern Canada. The sub-arctic continental climate is characterized by a large seasonal variation in temperature, low relative humidity and relatively low precipitation. Mean annual temperature is –3°C, with summer and winter monthly ranges of 5°–15°, and –10° – –20° C, respectively. Summer and winter extremes of 25° and –40° C are not uncommon. Mean annual precipitation is 300–400 mm per year with approximately 40 percent falling as snow. With a general northeasterly aspect, elevations range from 800 to 2250 m with the median elevation at 1325 m. Wolf Creek is situated within the Boreal Cordillera ecozone (Environment Canada, 1995) and consists of three principle ecosystems; boreal forest, shrub-tundra and alpine tundra with proportions of 22%, 58% and 20% respectively of the total basin area (Figure 1). The shrub tundra zone is snow-covered from early October to May with snowdrifts persisting until June. Wolf Creek is typical of headwater basins in the mountains of north-western Canada and was used in the Mackenzie Global Energy and Water Cycle Experiment (GEWEX) Study (MAGS) to characterize hydrometeorological processes for high elevations in the Mackenzie River basin.

The field site in Wolf Creek was near 1400 m a.s.l. in the Granger Creek sub-basin. The primary vegetation is shrub tundra, consisting mainly of 0.5 to 3 m high alder (*Alnus crispa*) shrubs overlying a ground cover of grasses and mosses. Shrubs of limited height (less than 1 m) may become completely buried in high snowfall years and become exposed during the melt season both gradually (as snow ablates) and rapidly (by spring-up of buried branches). A 30 m × 30 m (900 m^2) study grid of tall discontinuous shrub cover and melting snow was selected in the valley-bottom area of Granger Basin, and intensive field measurements were conducted there during the 2003 and 2004 melt seasons. Oblique photographs of the area were taken from the valley side, looking across the grid along a bearing of 200°, at regular intervals during the 2004 melt period (Figure 2). An aerial photograph was also taken on day 129 of 2004 (8th May) using a remote-controlled helicopter flying at an altitude of approximately 40 m (Figure 3).
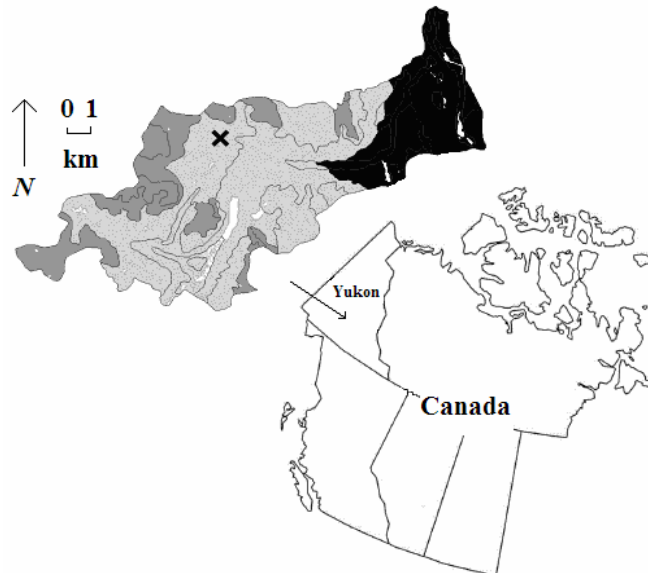

Figure 1. Location of the the Wolf Creek Research Basin.
Ecosystems shown include shrub tundra (in light grey), alpine tundra (in dark grey),
and boreal forest (in black). Lakes are shown in white, and the location of the study grid is
indicated by the cross. The individual contours represent the boundaries of individual sub-basins.
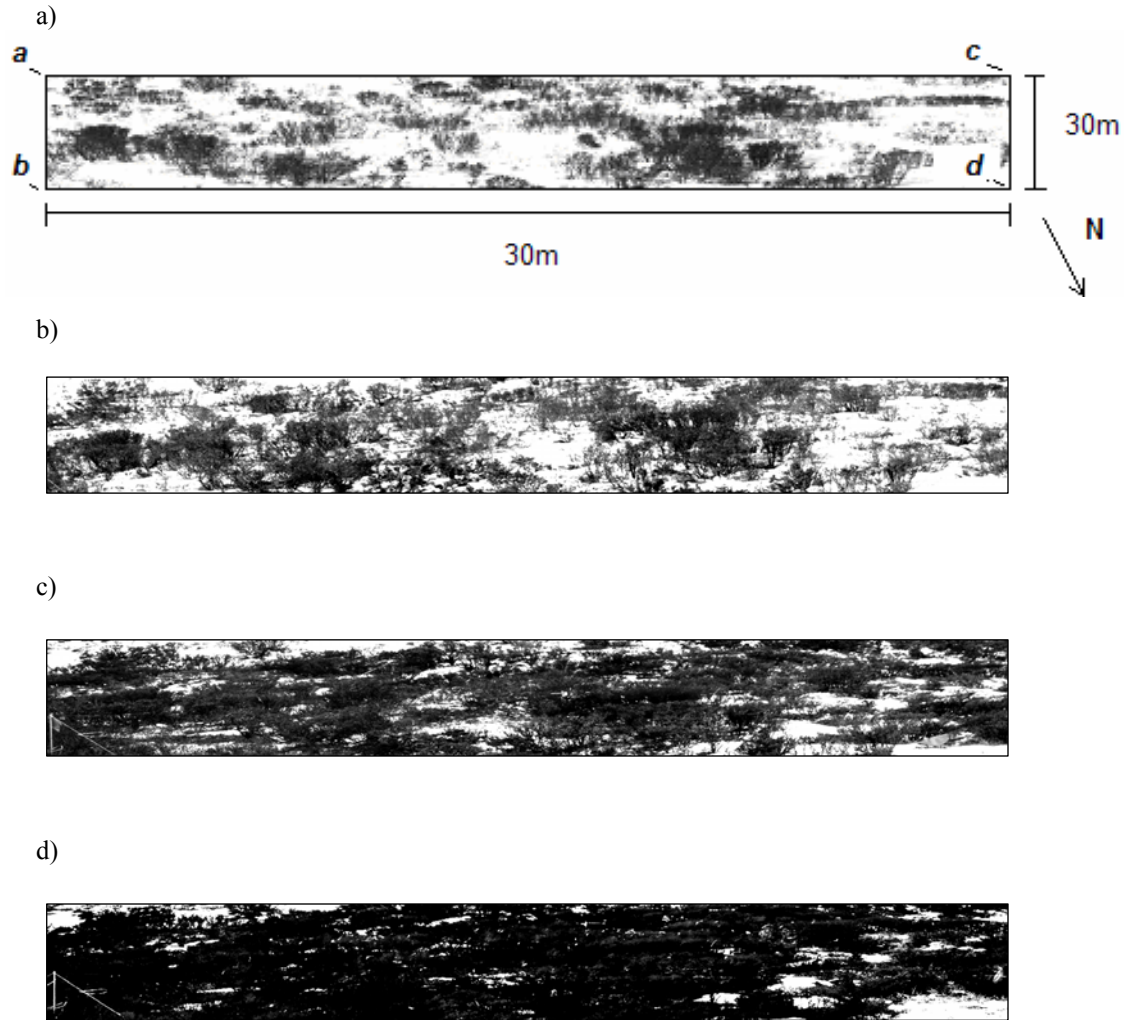
a)

b)

c)

d)

Figure 2. Oblique photo images of the 30m x 30 m study grid, showing snow patches (in white) and shrub patches (in greyscale), shown here for days (a) 112, (b) 122, (c) 129 and (d) 133. Figures a–d (corners of the photos) are shown to locate the position of the aerial photo (Figure 3).

The study grid was subdivided into 5 m × 5 m cells for measurement of canopy structure and snow depth. At the nodes of this grid, snow depth was measured at regular intervals, and plant area index PAI (the ratio between the total plant surface area and the surface area of ground that is covered by the plant) and sky-view factor v_f (the fraction of overlying hemisphere occupied by sky) were calculated from upward-looking hemispherical photographs using the Gap Light Analyzer (GLA) software (Frazer *et al.*, 1997). These photographs were taken at three stages during melt (days 112, 122 and 133 in 2004; 21st April, 1st May and 12th May, respectively). After the main melt period when the shrubs were fully exposed, four shrubs were selected at random in each cell and measured for maximum height (H) and width (W).

Solar irradiance was measured at the snow surface beneath shrubs of varying height and density in both the 2003 and 2004 melt periods. In 2003, eight upward-looking Matrix pyranometers were placed in and around four different shrubs of PAI 0.5–1.1 and 1.0–2.3 m height, and a further upward-looking Matrix pyranometer was placed above the canopy; this arrangement permitted

112

calculation of the transmission of shortwave irradiance through shrubs. The Matrix pyranometers had been previously calibrated against each other. In 2004 a single Kipp and Zonen CM21 pyranometer was placed above-canopy, and two Kipp and Zonen CNR1 (incoming and outgoing short and longwave) radiometers were placed at different sub-canopy locations between days 97–137. Because of changing solar direct beam path (12° increase in maximum solar elevation) through the canopy over this period, a 'virtual array' of three pyranometers, one each for the beginning, middle and end of the observation period, was generated from both of these sub-canopy data. In both years, irradiance was measured every 10 seconds with a Campbell 23X datalogger and averaged over 30 minute periods.

Albedo was observed in 2003 using two of the Matrix pyranometers. An upward-looking pyranometer was placed above the canopy level to measure incoming shortwave radiation. Reflected radiation was measured with a downward-looking pyranometer, firstly positioned over a large pure snow patch with no exposed vegetation or nearby shrubs, and was then placed above a large mass of cut shrub branches, which densely covered the ground. From these observations the albedo of pure snow and of pure shrubs could be calculated.
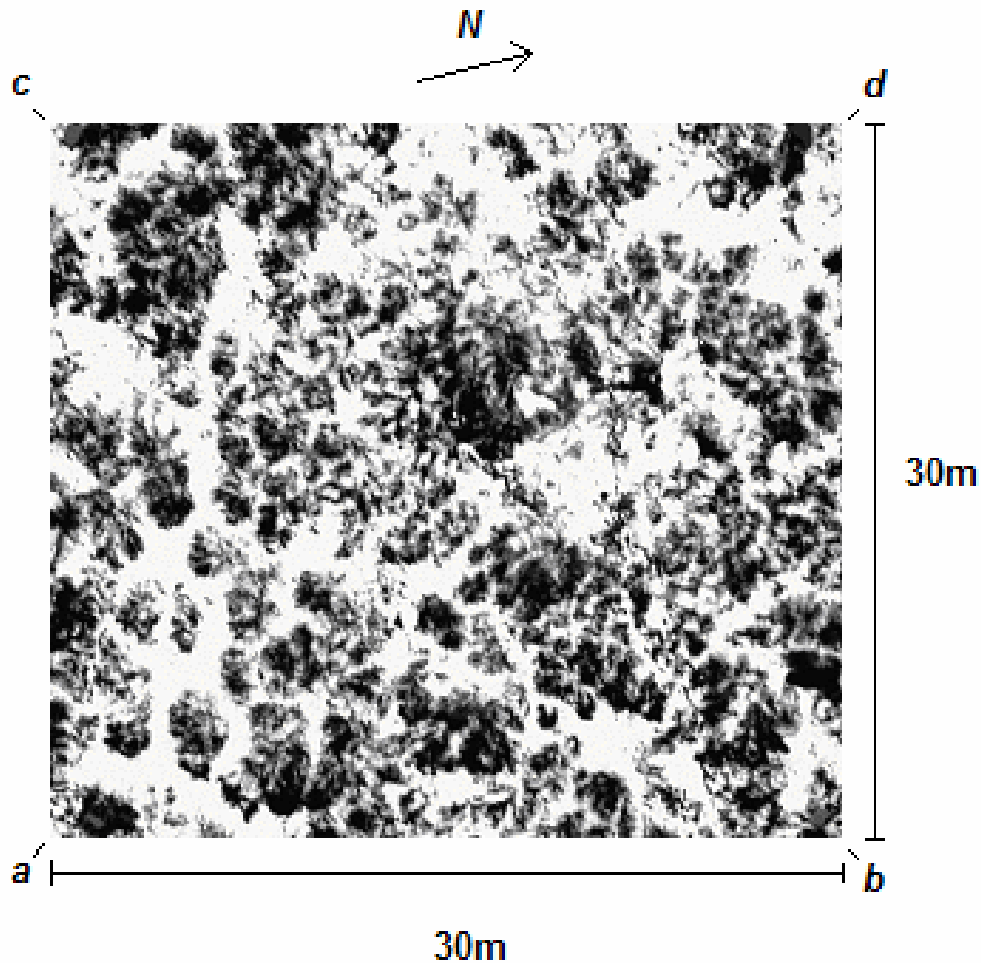

Figure 3. Aerial photo of the 30m x 30m study grid taken on day 129, showing snow patches (in white) and shrub patches (in greyscale). The figures a–d correspond with the same reference points in Figure 2.

FIELD RESULTS

Shrub density and sky view

GLA analysis of photographs within which branches extended into the majority of azimuth and zenith-angle bins were considered to represent shrub PAIs. The ten highest PAI values obtained for each observation date were averaged to assess changes in PAI resulting from increased shrub exposure as snow melted. Photographs where sky was visible in the majority of azimuth and zenith-angle bins were considered to represent canopy gaps; the highest 25 sky view factors (approximately 50% of the photographs) obtained on each date were averaged to give mean sky view factors for the gaps. Resulting values of PAI and v_f are given in Table 1.

Exposed shrub fractions

The location and fractional coverage of shrubs exposed above the snow were calculated from a vertical aerial photograph taken on day 129 (Figure 3). Shrubs were differentiated from snow patches and shadows on snow by applying a threshold to the image, giving a fractional coverage of 60% shrub and 40% snow. The results from an oblique image taken on the same day (Figure 2c), using the same classification, were 80% shrub and 20% snow; the shrub area is overestimated in oblique photographs because snow patches behind the shrubs are partially hidden from view.

A simple calibration method was applied to estimate the correct fractional areas from the remaining oblique images, taken on days 112, 122 and 133, by subtracting 20% from the shrub fractions and adding it to the snow fractions measured from these images. Estimated values of the correct exposed vegetation fraction F_v are presented for all dates in Table 1. Note that a snowcover was continuous under the canopy until day 133.

Table 1. Average and standard deviation values of PAI and v_f (where N > 1),
and F_v and τ values (N = 1) calculated for days 112, 122, 129 and 133 of 2004.

Day	112	122	129	133
PAI	0.45	0.51	0.62	0.62
(N=10)	±0.09	±0.10	±0.09	±0.09
v_f	0.77	0.70	0.59	0.59
(N=25)	±0.02	±0.04	±0.05	±0.05
F_v	0.22	0.41	0.60	0.69
τ	0.73	0.70	0.65	0.65

Shortwave transmission

The measured shortwave transmissivities from 10 radiometers (those placed centrally at the base of shrubs), representing the fraction of incident radiation penetrating to the snow surface beneath the canopy, were averaged and are shown in Figure 4 as a function of solar elevation angle θ. Two cases are shown: the first for a complete diurnal cycle under clear skies when the direct beam radiation dominated, and the second for a day with overcast skies when only diffuse light was present. Little relationship is observed between τ and θ for either period (R = 0.67 and 0.55, respectively), suggesting a horizontal orientation of the shrub branches (Ross, 1975). The variability in τ was higher under clear skies, as changes in solar elevation of only a few degrees were sufficient to cause rapid movement of shadows across the radiometer surfaces.

Shortwave albedo

The measured shortwave albedo of both the sunlit snow and shrub surfaces, representing the fraction of incident radiation reflected, was found to be 0.85 and 0.11 (variance 0.002 and 0.0005) respectively, when averaged over the daytime period of data collection.
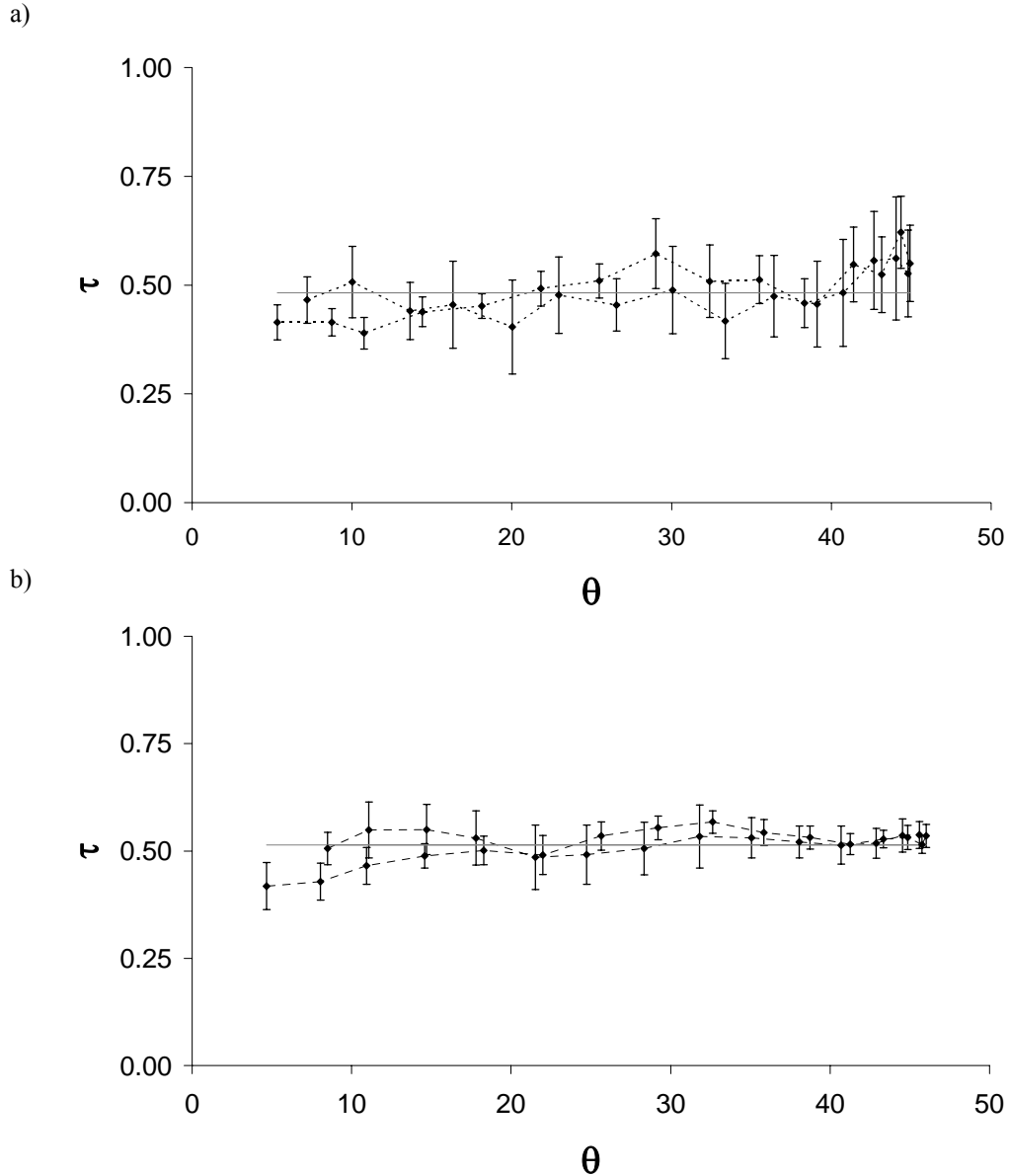
a)

b)

Figure 4. a) observed mean transmissivity (τ) of shortwave radiation for different solar elevation angles (θ) during a clear-sky diurnal period, with standard deviation indicated by error bar length. Modeled mean transmissivity is indicated by the straight line. (b) as in (a), but for an overcast diurnal period.

MODEL DESCRIPTIONS

Two-stream model

   Radiation schemes in atmospheric models and canopy schemes in land-surface models typically use a two-stream approximation representing vertical downwards and upwards fluxes of radiation. Heterogeneous land surfaces are often represented using tile models (e.g. Essery *et al.*, 2003) or dual-source models (e.g. Blyth *et al.*, 1999). Horizontal influences of shadows cast by a vegetation canopy onto an adjacent tile and multiple reflections between the tiles are not represented within the strictly vertical two-stream framework.

The two-stream model is that used in the dual-source model of Blyth *et al.* (1999) for sparse vegetation. The open fraction of the surface receives the full incident shortwave radiation $S_{\downarrow 0}$ without obstruction by vegetation. The shortwave radiation at the surface under the canopy comprises radiation transmitted through the canopy and multiple reflections between the snow and the overlying canopy, giving

$$S_{\downarrow v} = \frac{\tau(1-\alpha_v)}{1-\alpha_v\alpha_s}S_{\downarrow 0}, \tag{1}$$

where α_v is the vegetation albedo and α_s is the snow albedo. The parameterization of τ is described below. The areal average shortwave radiation at the surface for a landscape with shrub fraction F_v and open fraction $F_o = 1-F_v$ is then

$$S_{\downarrow AREAL} = F_o S_{\downarrow 0} + F_v S_{\downarrow v} \tag{2}$$

and the areal transmissivity for the landscape is

$$\tau_{AREAL} = \frac{S_{\downarrow AREAL}}{S_{\downarrow 0}}. \tag{3}$$

The upwards flux of radiation above the canopy is

$$S_{\uparrow v} = \left[\alpha_v + \frac{\tau^2(1-\alpha_v)^2\alpha_S}{1-\alpha_v\alpha_S}\right]S_{\downarrow 0}, \tag{4}$$

which includes radiation reflected direct from the canopy and radiation penetrating back through the canopy after multiple reflections from the surface.

Shading model

The radiative transfer model developed here is intended to more faithfully simulate the transmission of shortwave radiation to a snowpack masked by a discontinuous shrub canopy by including the influences of shrub shadows cast onto snow between shrubs and multiple reflections between snow in the gaps and the canopy. Three landscape segments are recognized in the model, as shown in Figure 5, and a unique description of shortwave transmission and reflectance is specified for each segment. Shrub patches cover fraction F_v of the surface and are semi-transparent, allowing some light to penetrate through the canopy to the snow surface below. Shadows cast by these shrub patches on adjacent snow-covered canopy gap areas cover fraction F_s, and the remaining sun-lit portions of the canopy gaps cover fraction $F_l=1-F_s-F_v$. The transfer schemes applied to each are described below.

Incoming radiation above the canopy is divided into a direct-beam component $S_{\downarrow B}$ and a diffuse component $S_{\downarrow D}$, giving $S_{\downarrow 0} = S_{\downarrow B} + S_{\downarrow D}$. The illuminated snow fraction initially receives the full direct component and diffuse radiation from the visible part of the sky, giving

$$S_{\downarrow l} = S_{\downarrow B} + v_f S_{\downarrow D} \tag{5}$$

which, after a single canopy reflection, is then

$$S_{\downarrow l} = (1-v_f)\alpha_v\alpha_s\left(S_{\downarrow B} + v_f S_{\downarrow D}\right), \tag{6}$$

and after a series of infinite reflections between snow and shrub, becomes

$$S_{\downarrow l} = \frac{1}{1-(1-v_f)\alpha_v\alpha_s}\left(S_{\downarrow B} + v_f S_{\downarrow D}\right). \tag{7}$$

The contribution of the radiance incident initially on the F_s fraction and then reflected to F_l is neglected, since it is a product of the shrub albedo and shrub view factor of the snow surface, both of which are small in this study.

In the shaded fraction, the snow is only illuminated by diffuse radiation from the sky and radiation passing through the vegetation, giving

$$S_{\downarrow s} = \frac{1}{1-(1-v_f)\alpha_v\alpha_S}v_f S_{\downarrow D}. \tag{8}$$

Shortwave radiation at the snow surface beneath the vegetation is given by the same expression as in the two-stream model, assuming that $S_{\downarrow B}$ and $S_{\downarrow D}$ are transmitted equally, so that

116

$$S_{\downarrow v} = \frac{\tau(1-\alpha_v)}{1-\alpha_v \alpha_s}\left(S_{\downarrow B} + S_{\downarrow D}\right). \tag{9}$$

τ is estimated as

$$\tau = e^{-f}, \tag{10}$$

where f is a bulk canopy optical thickness, which depends on solar geometry and canopy density and structure. Models differ in how they calculate f (e.g. Yamazaki *et al*. 1992, Pomeroy and Dion, 1996), but generally assume that it is linear in PAI, giving $f = K$ PAI. The extinction coefficient K then depends on θ, path length through the canopy and canopy structure. For a continuous canopy of height H, as considered in most models, the path length l is

$$l = \frac{H}{sin\,\theta}, \tag{11}$$

however this is not the case for the discontinuous canopy considered here. Instead, we derive an effective K from the τ data (Figure 4) and the average PAI result of the shrubs from where this data was obtained, where

$$K = -\frac{1}{\overline{PAI}}ln\,\overline{\tau}. \tag{12}$$

Values of K show no dependency on θ, and mean values are 0.84 and 0.91 for clear and overcast sky conditions, respectively. When substituting these coefficients back into Equation (10), the resulting τ (indicated by the grey line in Figure 4) matches closely to that observed, where root-mean-squared errors are 0.055 and 0.033 for clear and overcast conditions, respectively. The mean of these coefficient values (0.875) is applied within the model, such that

$$\tau = e^{-0.875\ PAI}. \tag{13}$$

There may be site specific variations in the effective K and further work is necessary to evaluate extinction as a function of shrub geometry, length scale, stem angle and solar angle in sparse canopies. Note that Equation (13) is also applied within the two-stream model.

Weighting the irradiance calculated for each snow surface segment by the fractional areas which they cover, the average irradiance at the snow surface is obtained as

$$S_{\downarrow AREAL} = F_l S_{\downarrow l} + F_s S_{\downarrow s} + F_v S_{\downarrow v} \tag{14}$$

and the areal transmissivity is

$$\tau_{AREAL} = \frac{S_{\downarrow AREAL}}{S_{\downarrow B} + S_{\downarrow D}}. \tag{15}$$

The shortwave radiation reflected from the vegetated fraction is given by Equation (4), and the reflected radiation from the illuminated and shaded gap fractions are simply

$$S_{\uparrow l} = \alpha_s S_{\downarrow l} \tag{16}$$

and

$$S_{\uparrow s} = \alpha_s S_{\downarrow s}. \tag{17}$$

Finally, the average shortwave radiation reflected from the landscape is the weighted sum

$$S_{\uparrow AREAL} = F_l S_{\uparrow l} + F_s S_{\uparrow s} + F_v S_{\uparrow v}, \tag{18}$$

and the effective areal albedo is

$$\alpha_{AREAL} = \frac{S_{\uparrow AREAL}}{S_{\downarrow B} + s_{\downarrow D}} \tag{19}$$

Shaded areas are calculated using a method similar to that suggested by Granberg (1988) for forest shading. Shrubs are divided into horizontal slices (of width equal to the shrub widths determined from image analysis) that are then projected along the direction of the solar beam until they intersect the surface. Shadows are defined by the projections of the shrubs on the surface. This shaded snow adjacent to and under the exposed shrubs is then given an effective albedo of 0.75 based on the work of Melloh *et al*. (2002) and Hardy *et al*. (1998). Note that this effective value is lower than was measured in the field under sunlit conditions for segment F_l.
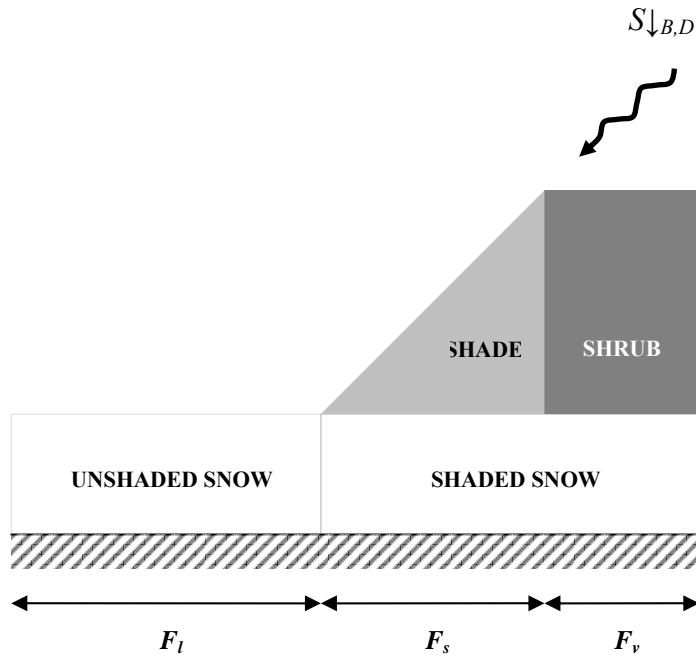
117

Figure 5. Diagrammatic representation of the shadow model, showing each of the three land segments and their respective snow shading condition.

MODEL RESULTS

Shaded areas

Simulations were performed using the parameter values derived from observations (Table 1) for days 112, 122, 129 and 133 in 2004. The radiative transfer model was run using a grid of shrub heights with the same ~3.5 cm pixel size as the aerial photograph shown in Figure 3. Since an aerial photograph was only available for day 129 and heights were only measured for a sample of 144 shrubs, methods were required to construct complete grids of vegetation cover and height for each date.

Measured shrub heights were interpolated by kriging across the entire study grid area to generate a maximum height field. The positions of exposed shrubs, known from the day 129 aerial image, were manufactured for other dates by contracting (for days 112 and 122) or expanding (for day 133) the shrub patches present in the aerial image. This was done by changing the digital brightness threshold for shrub to non-shrub applied to the image to fit the calibrated exposed shrub fraction, F_v, calculated for each date (Table 1). Exposed shrub heights were simulated by linearly reducing the interpolated height field by area-average snow depths measured on the dates nearest to those on which the oblique photographs were taken.

Shaded areas of snow adjacent to the shrub patches were calculated with appropriate solar elevations and azimuths at half-hourly intervals to obtain diurnal variations in shading lengths. Figure 6 shows simulated shadows and exposed shrubs for days 112 and 133 at 1300h (local solar noon) when the shaded fraction is minimized and the maximum extent of illuminated canopy gaps is reached. The landscape progresses from a gap-dominated environment before melt commences to a shrub-dominated environment as the shrubs are progressively exposed by the receding snowpack. This transition occurred at some point between days 122 and 129 in 2004.

a)   b)
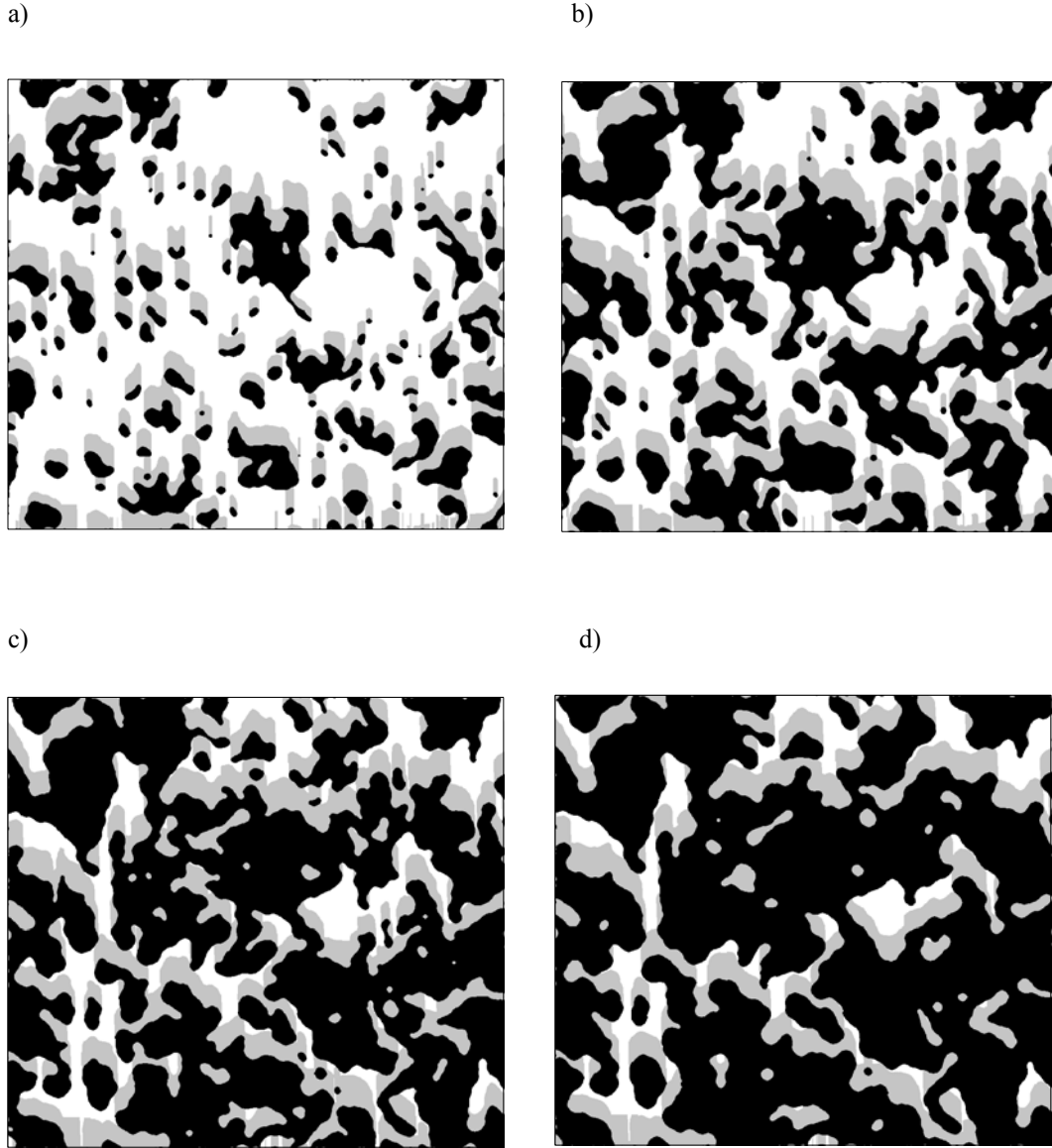

c)   d)

Figure 6. Model simulated areas of illuminated snow (in white), shaded snow (in grey), and exposed shrub (in black), shown here at 13:00 (local solar noon) for days (a) 112, (b) 122, (c) 129 and (d) 133 under clear-sky conditions. Note that the scale and positioning is identical to that of the aerial photo (Figure 3).

Figure 7 shows calculated gap shaded fraction F_s and illuminated fraction F_l as a function of solar elevation θ for days 112 and 133. F_l approaches zero when the shrubs cast long shadows at low θ. On day 112, when the shrubs still have small exposed areas and heights above the snowpack, F_l rises rapidly after the sun rises above the horizon, and sun-lit snow patches dominate the landscape for $\theta \geq 22°$. A maximum of $F_l = 0.58$ is obtained at solar noon, at which time $F_s = 0.21$. On later dates, as the exposed shrubs increase in abundance and height, a recession of the canopy gap area naturally decreases the values of both F_l and F_s, and by day 133 F_l has become an insignificant fraction of the landscape ($F_l = 0.1$ at solar noon). It follows that canopy gaps remaining during the latter stages of melt are increasingly shaded by the shrubs.
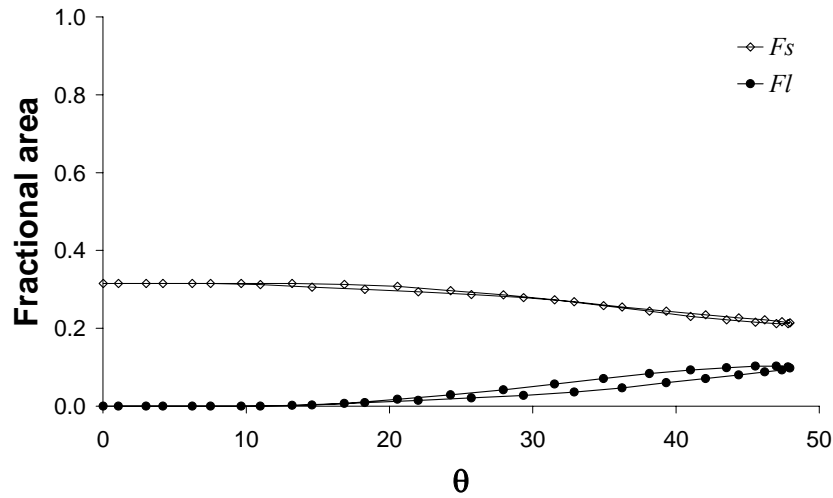
a)
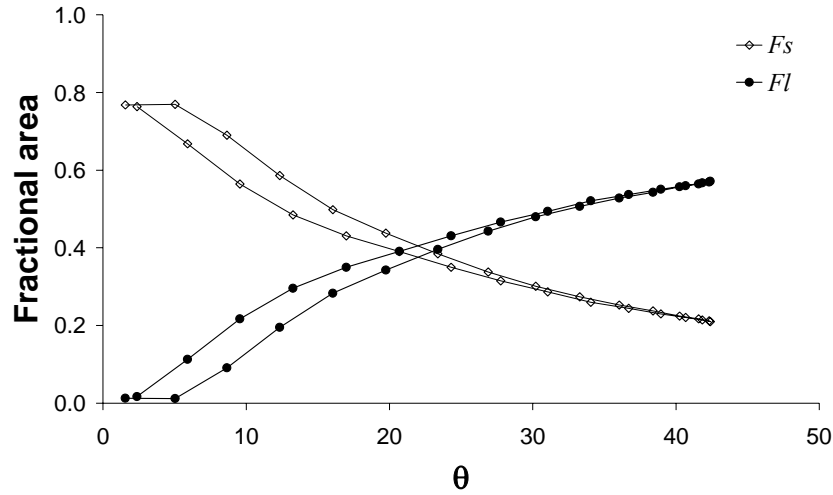
b)

Figure 7. a) fractional areas of shaded and illuminated snow (F_s and F_l, respectively)
for different θ on day 112; b) as for (a), for day 133.

Areal transmissivity

Figure 8 shows τ_{AREAL} on days 112 and 133, as simulated by both shading and two-stream models using measured $S_{\downarrow 0}$ data from day 121 (a clear-sky period, in which the direct beam fraction is assumed 90% of $S_{\downarrow 0}$ throughout). On day 112, the two-stream model simulates a high τ_{AREAL} result (0.92) since 78% of the landscape consists of canopy gap areas (where $\tau = 1.0$), and the remaining exposed shrub fraction has a high transmissivity due to the low pre-melt PAI. In the shading model, τ_{AREAL} is initially very low (0.22 for $\theta \leq 5°$) when the canopy gaps are almost entirely shaded. It follows that for shorter shadow lengths associated with higher θ, less radiation extinction by the canopy occurs, τ_{AREAL} reaches 0.73 at solar noon ($\theta \leq 42°$), and τ_{AREAL} would tend further towards (but not exactly to) the two-stream result if θ were higher. Over the course of day 112, in which 24.5 MJ m^{-2} of (cumulative) $S_{\downarrow 0}$ is measured, the two-stream model simulates

22.7 MJ m^{-2} of shortwave radiation transmitted to the snow surface, compared to 15.8 MJ m^{-2} by the shading model (for which the flux-weighted average τ_{AREAL}, as used hereinafter, is 0.64).

When using measured $S_{\downarrow 0}$ data from an overcast-sky period (day 122; diffuse fraction assumed 100% throughout the day) to run the models, the shading model simulates the transmission of diffuse light equally over the canopy gaps. The transmissivity through F_v remains unchanged from the clear-sky simulation (0.66), since in this segment the model transmits diffuse and direct light identically, and average τ_{AREAL} remains constant at 0.76. The two-stream model in effect transmits global radiation for all segments, and the τ_{AREAL} result of 0.92 is therefore unchanged from the clear-sky simulation. 9.5 MJ m^{-2} of shortwave radiation is transmitted to the snow surface by the shading model, compared to 11.5 MJ m^{-2} by the two-stream model and 12.5 MJ m^{-2} measured above the canopy.

By day 133, the diurnal range of τ_{AREAL} simulated by the shading model in clear-sky conditions is reduced significantly from day 112, due to the extensive F_v fraction (69%) and the resulting reduction of canopy gaps with variable shaded and illuminated fractions. For $\theta \leq 9°$, τ_{AREAL} is actually higher on day 133 than on day 112, since the reduction in F_s (and associated beam extinction) relative to day 112 more than offsets the increased reduction of global irradiance below the shrubs (due to enhanced shrub abundance and density). Thereafter, τ_{AREAL} rises from 0.40 at low θ to 0.50 at solar noon (average 0.47), and 11.5 MJ m^{-2} of shortwave radiation is transmitted to the snow surface (73% of the amount on day 112). The two-stream model simulates a constant τ_{AREAL} of 0.70, and 17.3 MJ m^{-2} are transmitted (76% of the respective day 112 value). For the overcast simulation, 7.3 MJ m^{-2} and 8.8 MJ m^{-2} are transmitted by the shading and two-stream models, respectively, in which τ_{AREAL} is 0.58 and 0.70.
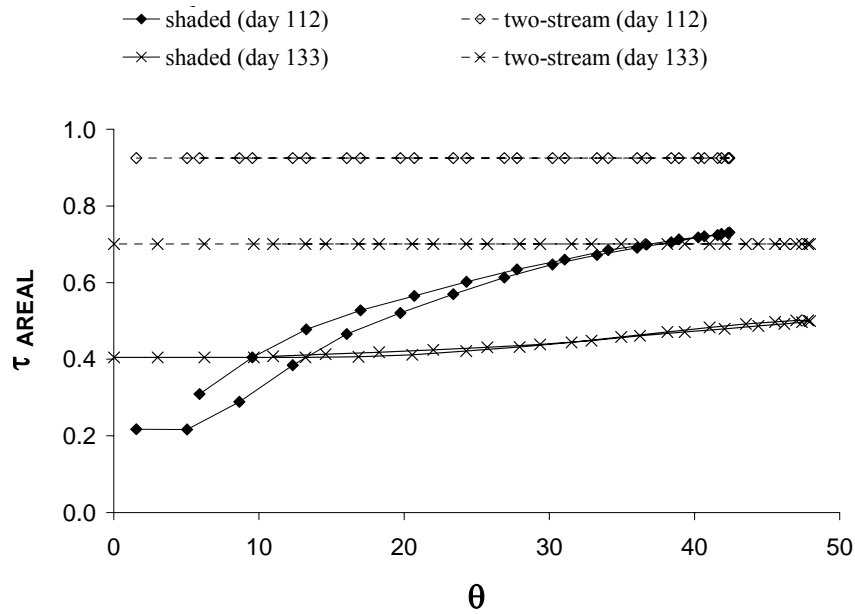

Figure 8. Simulated areal transmissivity (τ_{AREAL}) for different θ using the shading and two-stream models for days 112 and 133 under clear-sky conditions.

Areal albedo

Figure 9 shows α_{AREAL} on days 112 and 133 for clear-sky conditions. On day 112, α_{AREAL} rises rapidly from 0.14 at low θ to 0.59 at solar noon (average 0.51), representing the increase of illuminated canopy gaps at the expense of those shaded, in which the beam fraction is extinguished and not available for reflection. The absence of shadows in the two-stream model produces a constant α_{AREAL} result of 0.75, which is only 0.10 below that of a purely illuminated snow landscape, since the exposed shrub segment remains small and moderately transparent (α = 0.41). By day 133, the shrub area and density has increased considerably, such that α has decreased to 0.33 for F_v and the shading model result of α_{AREAL} is now limited in diurnal range (0.24–0.32, average 0.29). The α_{AREAL} result from the shading model increases in overcast conditions (0.37), but the two-stream result of α_{AREAL} (0.49) holds for either clear or overcast conditions.
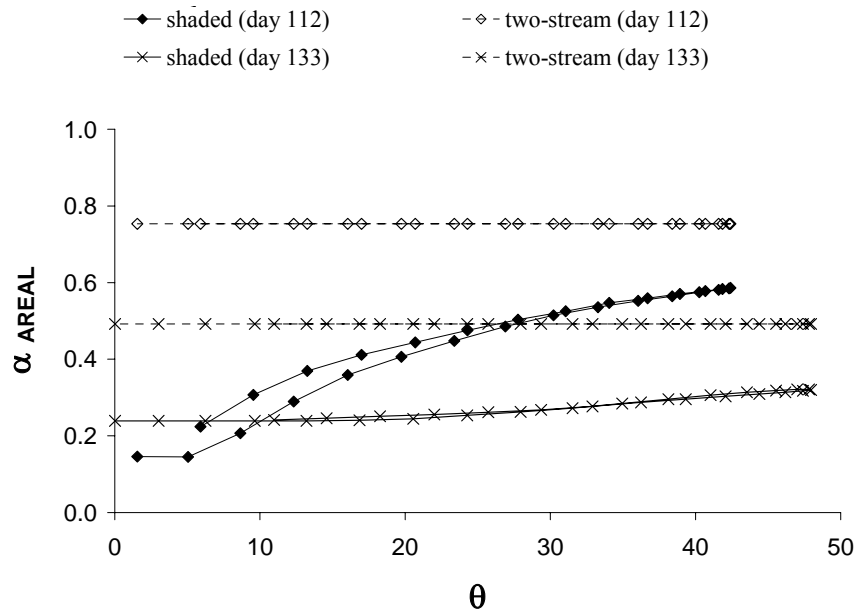

Figure 9. Simulated areal albedo (α_{AREAL}) using the shading and two-stream models for days 112 and 133 under clear-sky conditions.

Comparison with observations

It was not feasible in the field to deploy sufficient randomly spaced radiometers to verify the marked areal transmissivities and albedo described above as estimated using the shading model. However, whilst not an attempt at model verification, there were sufficient subcanopy radiometers deployed in 2003 to generate an observed τ_{AREAL} with which to compare the derived trends against those generated from the model. An average irradiance under the canopy was calculated for the clear-sky day 129 period in 2003, from the four radiometers placed centrally at the base of shrubs and a further four deployed to the side of shrubs and in canopy gaps. Figure 10 shows a comparison of this calculated τ_{AREAL} against the shading and two-stream model approximations of τ_{AREAL} using the parameter values for day 129 in 2004 (Table 1).

Results indicate that the observed (flux-weighted) average τ_{AREAL} (0.60) is lower than the corresponding two-stream result (0.76), but higher than the shading model result (0.48); potential reasons for the latter include an incorrect model specification of the exposed shrub fraction and its structural attributes (e.g. PAI) by assuming the same values for day 129 in 2003 and those actually

122

measured in the field one year later. However, the linear fit of observed τ_{AREAL} shows a clear increasing trend with θ, where the slope coefficient (0.0034) is almost identical to that of the linear fit from the shading-model (0.0031), and the root-mean-squared error between observed and shading-model τ_{AREAL} (0.13) is lower than for the two-stream model (0.21). These results provide the first indication of the increased physical reality with which the shading-model can simulate the processes of shortwave transmission (and potentially reflection) from a discontinuous shrub canopy, relative to a two-stream approximation.
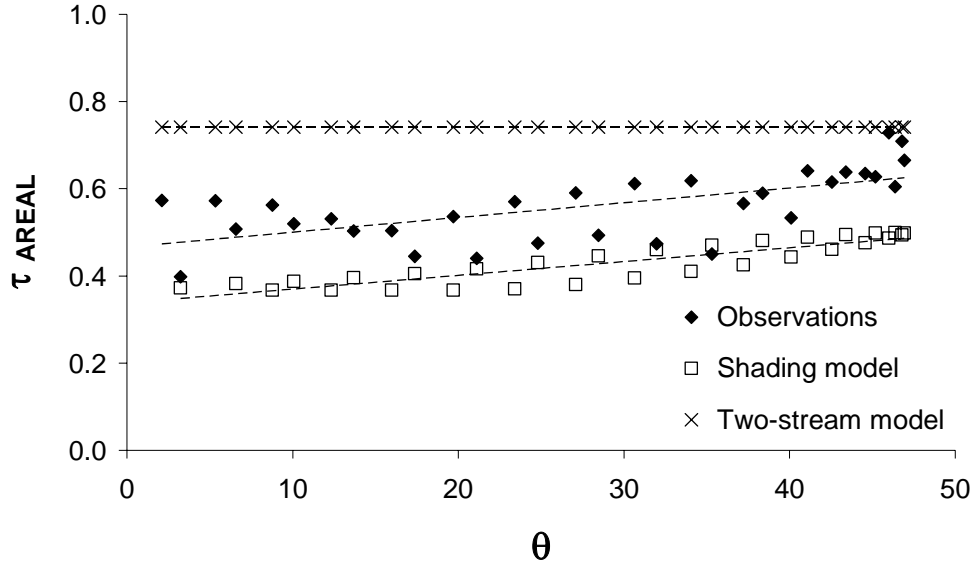

Figure 10. Shading and two-stream model simulations of τ_{AREAL} for day 129 2003, against the observed τ_{AREAL} from 9 subcanopy radiometers on this date.

PARAMETERIZATION OF SHADOW FRACTIONS

The shading model described above predicts patterns of shadow over a landscape with discontinuous shrub cover, but it is very computationally expensive and requires a detailed map of shrub heights. For practical applications, a parameterization giving a rapid calculation of the shaded fraction of the landscape from a small number of parameters is required.

Consider a shrub of height H and width W. The length of the shadow cast by this shrub when the sun is at elevation θ is $l = H/\tan\theta$. If l exceeds the gap distance L to the next shrub in the shaded direction, the shrub shadows overlap. The fraction of the landscape covered by shadows in gaps is

$$f_S = \frac{\bar{l}}{\overline{W} + \overline{L}}, \tag{20}$$

where $\bar{l}$, $\overline{W}$ and $\overline{L}$ are the averages of l, W and L over the landscape. Allowing for overlap of shadows, the average shadow length is given by

$$\bar{l} = \iint dH\, dL\, p(H,L)\, min\left(\frac{H}{\tan\theta}, L\right), \tag{21}$$

where $p(H,L)$ is the joint probability distribution of H and L. From the surveyed shrub heights and gap lengths measured from the aerial photograph, it is found that H and L are uncorrelated, so the joint distribution can be replaced by the product $p(H)p(L)$ for the individual distributions of H and L. Moreover, it is found that the distributions can be approximated by a normal distribution for H and a lognormal distribution for L, giving

123

$$p(H) = \frac{1}{\sqrt{2\pi}\sigma_H} exp\left[-\frac{(H - \overline{H})^2}{2\sigma_H^2} \right]$$ (22)

and

$$p(L) = \frac{1}{\sqrt{2\pi}L\sigma_y} exp\left[-\frac{(ln\,L - \overline{y})^2}{2\sigma_y^2} \right],$$ (23)

where σ_H and σ_L are the measured standard deviations of H and L,

$$\sigma_y^2 = ln\left[1 + \left(\frac{\sigma_L}{\overline{L}}\right)^2 \right]$$ (24)

and

$$\overline{y} = ln\,\overline{L} - \frac{\sigma_y^2}{2}\,.$$ (25)

Numerical integration of Equation (21) and substitution in Equation (20) then gives an efficient prediction of the shading fraction. Figure 11 compares this parameterization with results from the shading model for varying solar elevations using the vegetation grids for days 112 and 133.
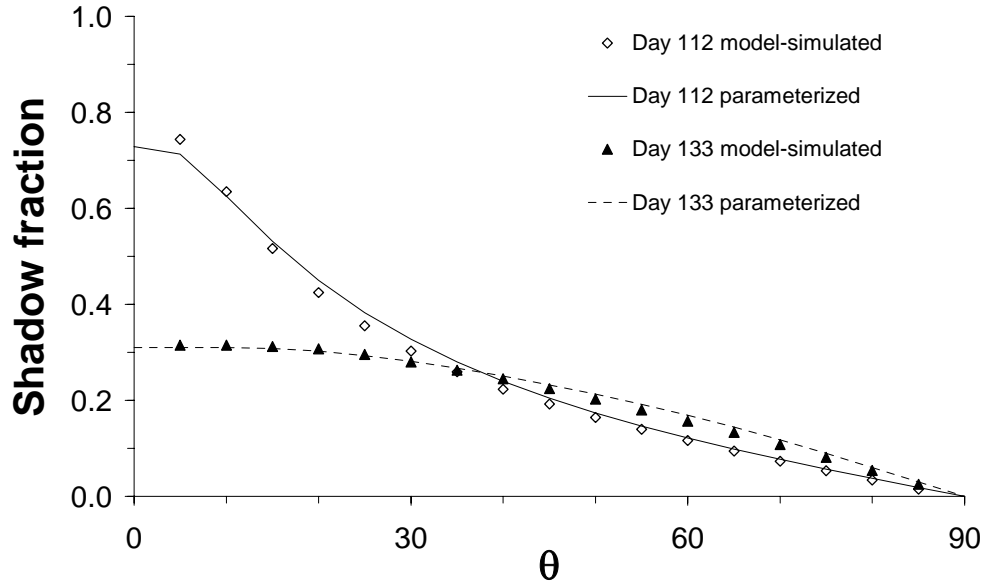

Figure 11. Fractional areas of the shaded snow segment (F_s) as calculated separately
by the shading model and parameterized form, for days 112 and 133.

DISCUSSION

The implications of the relationships presented here are that the transmission and reflectance of shortwave radiation are determined primarily as a function of solar elevation at the diurnal scale, and of the vegetated fraction of the landscape over the course of the melt season. At low solar elevation angles, even when the exposed shrub fractional area is sparse, such as in the premelt

period, the snowpack can be almost completely masked by the apparent canopy cover consisting of shrub bushes and the shadow areas that they cast. The shading model simulations of both effective landscape transmissivity and albedo are low at this stage, since a large proportion of incident direct radiation is extinguished by this apparent canopy coverage, and only a minor proportion reaches the snow surface or is reflected. At higher solar elevation angles, the apparent canopy cover decreases since shadow lengths are reduced, and the areal transmissivity and albedo increase. It follows that the disparity between these results and those from the two-stream model, in which the apparent canopy cover consists only of the vegetated fraction, narrows through the melt season as the progressive exposure of shrubs decreases the potential shaded canopy gap area, or under overcast sky conditions when canopy gaps are illuminated uniformly.

The parameterized version of the shading model can be run for discontinuous shrub canopies with only basic information about the canopy characteristics from which to simulate the shaded landscape fraction. An aerial photograph of the study area, of sufficiently high resolution to delineate individual shrub patches and canopy gaps, provides the most rapid method for obtaining this information. Image-analysis software programs (e.g. Sigmascan; Systat Inc.) can readily compute the required statistics and distributions of shrub width and gap length, and the shade lengths present in the image during clear-sky conditions can be inverted trigonometrically to derive the shrub height distribution. The latter might also be obtained from airborne LIDAR data, although shrub height data could be uncertain for shrubs where the signal penetrates beyond the bush top.

The default normal and lognormal distributions used for shrub height (H) and gap distance (L), respectively, can easily be replaced by alternative H and L distributions from other areas that are more appropriate. An important consideration is the landscape area over which the shading model is to be run, and the range of environmental controls of shrub placement present within this area (e.g. topography, drainage). For instance, fitting an exponential variogram to the study grid H distribution gives a range of 3.5 m, suggesting a random canopy structure on scales between this and the 30 m scale of the survey grid. However, at the larger scale of the valley (~500m), a clear spatial organization appears with taller shrubs being found in more sheltered areas and close to the stream, and the distribution may become increasingly skewed. Even at the microscale where the environmental controls of topography and drainage appear uniform, shrubs may not necessarily be located randomly across the landscape (Okin and Gillette, 2001).

CONCLUSIONS

The transmission of shortwave radiation through discontinuous shrub canopies to an underlying snowcover is a complex but important process that can significantly affect the amount and rate of snowmelt in this environment. Additionally, the proportion of incident shortwave radiation extinguished by the canopy and not reflected is critical to determining the atmospheric heat and moisture fluxes from this landscape. The effective shortwave radiation transmissivity and albedo of this landscape are substantially different from those in which a continuous shrub canopy exists or is absent althogether, since the apparent canopy coverage will vary considerably with solar elevation angle.

In this paper, a physically realistic model has been developed to simulate the effective transmission and reflectance of shortwave radiation from a landscape consisting of a discontinuous shrub canopy over a melting snowpack. The model parameterizes the transmission and reflectance of direct and diffuse shortwave radiation from three landscape segments, including a semi-transparent exposed shrub segment, and both an exposed and shaded canopy gap segment. The introduction of shaded canopy gaps sets the new radiative model apart from simpler radiative transfer models in which the landscape is represented by one or two static land classes, and it is believed that this method improves the diurnal simulation of shortwave transfer in this environment.

Results from this study indicate that early within the melt period, the direct shortwave radiation transmitted to the snow surface and reflected from the landscape increases considerably as the solar elevation angle increases, which reduces the shadow lengths across the canopy gaps and in turn the proportion of above-canopy irradiance that is extinguished within these areas. Areal transmissivity and albedo was up to 0.70 and 0.61 lower relative to that simulated by a two-stream approximation in which no shadows are considered. This effect is reduced at full shrub-exposure when the potential canopy gap area for shading is small; this reinforces the importance of representing shadows within radiation transfer schemes for the shrub environment.

To calculate areal transmissivity and albedo for shrub tundra, the shaded landscape fraction can be determined using a parameterized version of the shading model. The height and gap length distributions and the statistics required for this calculation can be obtained from high resolution remote imagery, field surveys or informed assumptions. The shrub transmission and snow albedo parameterizations developed within the radiative transfer component of the model may, however, warrant further investigation before use operationally, and future work extending from this study should address these issues initially. For instance, an improved spatially-variable snow albedo scheme to estimate the effects of shrub canopy extinction on shaded snow albedo, and of buried branches on albedo is needed. Also, the extinction coefficients should be parameterized differently for discontinuous shrub canopies, to account for such factors as the effect of shrub and gap dimensions on path length through the canopy.

Finally, a caveat, that the areal albedo and transmissivities estimated using the shading model, though physically reasonable and consistent with available observations, have not been verified by areal observations in this study. The practical reason for this is that it was not feasible to deploy sufficient randomly spaced radiometers to verify such a marked spatial distribution of transmission and reflectance. Ultimately the shortwave radiation scheme will need testing as part of a comprehensive energy balance model for shrub snowmelt, where changes in areal snow mass can be used to evaluate model performance.

REFERENCES

Blyth EM, Harding RJ, Essery R. 1999. A coupled dual source GCM SVAT. Hydrology and Earth System Science 3: 71–84.

DeFries R, Hansen M, Townshend JRG, Sholberg R. 1998. Global land cover classifications at 8km spatial resolution: The use of training data derived from Landsat imagery in decision tree classifiers. International Journal of Remote Sensing 19: 3141–3168.

Environment Canada. 1995. Terrestrial Ecozones of Canada. Ecological Land Classification Series No. 19, Ottawa.

Essery RLH, Best MJ, Betts RA, Cox PM, Taylor CM. 2003. Explicit representation of subgrid heterogeneity in a GCM land-surface scheme. Journal of Hydrometeorology 4: 530–543.

Essery RLH, Pomeroy JW. 2004. Implications of spatial distributions of snow mass and melt energy on snowcover depletion: theoretical considerations. Annals of Glaciology 38: 261–265.

Epstein HE, Beringer J, Gould WA, Lloyd AH, Thompson CD, Chapin FS, Michaelson GJ, Ping CL, Rupp TS, Walker DA. 2004. The nature of spatial transitions in the Arctic, Journal of Biogeography 31: 1917–1933.

Frazer GW, Canham CD, Lertzman KP. 1999. Gap Light Analyzer GLA, Version 2.0: Imaging Software to Extract Canopy Structure and Gap Light Transmission Indices from True-color Fisheye Photographs, Users Manual and Program Documentation. Burnaby, British Columbia: Simon Fraser University, and Millbrook, NY: Institute of Ecosystem Studies. 1–40 pp.

Granberg HB. 1988. A forest shading model using bit-mapped graphics. Agricultural and Forest Meteorology 43: 225–234.

Gryning SE, Batchvarova E, de Bruin HAR. 2001. Energy balance of a sparse coniferous high-latitude forest under winter conditions. Boundary-Layer Meteorology 99: 465–488.

Hardy JP, Davis RE, Jordan R, Ni W, Woodcock CE. 1998. Snow ablation modeling in a mature aspen stand of the boreal forest. Hydrological Processes 12: 1763–1778.

Huntingford C, Allen SJ, Harding RJ. 1995. An intercomparison of single and dual-source vegetation-atmosphere transfer models applied to transpiration from Sahelian savanna. Boundary-Layer Meteorology 74: 397–418.

Jia GJ, Epstein HE, Walker DA. 2003. Greening of the Alaskan Arctic over the past two decades. Geophysical Research Letters 30: 2067.

Jorgenson T, Heiner M. 2004. Ecosystems of Northern Alaska. Unpubl. Rep. by ABR, Inc., Fairbanks, AK.

Koivusalo H, Kokkonen T. 2002. Snow processes in a forest clearing and in a coniferous forest. Journal of Hydrology 262: 145–164.

Lee YH, Mahrt L. 2004. An evaluation of snow melt and sublimation over short vegetation in land surface modelling. Hydrological Processes 18: 3543–3557.

McCartney SE, Carey SK, Pomeroy JW. 2005. Spatial variability of snowmelt hydrology and its controls on the streamflow hydrograph in a subarctic catchment, Hydrological Processes: this issue.

Melloh RA, Hardy JP, Bailey RN, Hall TJ. 2002. An Efficient Snow Albedo Model for the Open and Sub-Canopy. Hydrological Processes 16: 3571–3584.

Natural Environmental Research Council. 2005. Climate change-scientific certainties and uncertainties. NERC Press, Swindon, UK.

Ni W, Li X, Woodcock C, Roujean JL, Davis RE. 1997. Transmission of solar radiation in boreal conifer forests: measurements and models. Journal of Geophysical Research 102 (N24): 29555–29566.

Nijssen B, Lettenmaier DP. 1999. A simplified approach for predicting shortwave radiation transfer through boreal forest canopies. Journal of Geophysical Research 104: 27859–27868.

Okin GS, Gillette DA. 2001. Distribution of vegetation in wind-dominated landscapes: Implications for wind erosion modeling and landscape processes. Journal of Geophysical Research 106: 9673–9683.

Pomeroy JW, Dion K. 1996. Winter Radiation Extinction and Reflection in a Boreal Pine Canopy: Measurements and Modelling. Hydrological Processes 10, 1591–1608.

Pomeroy JW, Granger RJ. 1997. Sustainability of the western Canadian boreal forest under changing hydrological conditions—I- snow accumulation and ablation. In Rosjberg D, Boutayeb N, Gustard A, Kundzewicz Z, Rasmussen P. (ed.) Sustainability of Water Resources under Increasing Uncertainty. IAHS Publication No. 240. IAHS Press: Wallingford, UK, pp. 237–242.

Pomeroy JW, Bewley DM, Essery RLH, Hedstrom N, Granger RJ, Sicart RE, Janowicz R. 2005. Shrub tundra snowmelt. Hydrological Processes: this issue.

Raupach MR, Finkele K, Zhang L. 1997. SCAM Soil-Canopy-Atmosphere Model: Description and Comparisons with Field Data. CSIRO CEM Tech Report No. 132, pp. 1–81.

Ross J. 1975. Radiative Transfer in Plant Communities. In Monteith JL (ed.) Vegetation and the Atmosphere, Academic Press, London, pp. 13–55.

Roujean JL. 1999. Two-story equations of transmission of solar energy TSETSE in open boreal conifer tree stands. Journal of Geophysical Research 104 (D22): 27869–27879.

Shuttleworth WJ, Wallace JS. 1985. Evaporation from sparse crops-an energy combination theory. Quarterly Journal of the Royal Meteorological Society 111: 839–855.

Strack JE, Pielke RA, Adegoke J. 2003. Sensitivity of Model-Generated Daytime Surface Heat Fluxes over Snow to Land-Cover Changes. Journal of Hydrometeorology 4: 24–42.

Sturm M, Racine C, Tape K. 2001. Increasing shrub abundance in the Arctic. Nature 411: 546–547.

Sturm M, Schimel J, Michaelson G, Welker JM, Oberbauer SF, Liston GE, Fahnestock J, Romanovsky VE. 2005. Winter Biological Processes Could Help Convert Arctic Tundra to Shrubland. BioScience 55: 17–26.

Viterbo P, Betts AK. 1999. Impact on ECMWF forecasts of changes to the albedo of the boreal forests in the presence of snow. Journal of Geophysical Research 104 (D22): 27803–27810.

Woo MK, Giesbrecht M. 2000. Simulation of snowmelt in a subarctic spruce woodland: 1. tree model. Water Resources Research 36: 2275–2285.

Yamazaki T, Kondo J, Watanabe T. 1992. A heat-balance model with a canopy of one or two layers and its application to field experiments. Journal of Applied Meteorology 31: 86–103.